IEEE Access
Multidisciplinary | Rapid Review | Open Access Journal

Received August 8, 2017, accepted August 24, 2017, date of publication September 12, 2017, date of current version November 14, 2017.

Digital Object Identifier 10.1109/ACCESS.2017.2751498

A Wideband Differential-Fed Dual-Polarized Microstrip Antenna Under Radiation of Dual Improved Odd-Order Resonant Modes

NENG-WU LIU, (Student Member, IEEE), LEI ZHU, (Fellow, IEEE), XIAO ZHANG, (Student Member, IEEE), AND WAI-WA CHOI, (Senior Member, IEEE)

Department of Electrical and Computer Engineering, Faculty of Science and Technology, University of Macau, Macau, China

Corresponding author: Neng-Wu Liu (yb47448@umac.mo)

This work was supported in part by the National Natural Science Foundation of China through General Program under Grant 61571468, in part by the University of Macau under Multi-Year Research Program under Grant MYRG2017-00007-FST and Grant MYRG2015- 00010-FST, and in part under the Grant CPG2017-00028-FST.

ABSTRACT A low profile differential-fed dual-polarized microstrip patch antenna (MPA) with bandwidth enhancement is proposed under radiation of the first and second odd-order resonant modes. First, all of even-order modes are fully suppressed by using a differentially feeding scheme instead of the single probe feed. Next, the radiation pattern of a square MPA is theoretically analyzed. It is demonstrated that the traditional monopole-like radiation of the second odd-order mode in the H-plane, i.e., TM_{21} mode, can be transformed into the broadside radiation by etching out a narrow slot at the center of the radiating patch. After that, an array of shorting pins is symmetrically embedded underneath the radiating patch so as to progressively push up the resonant frequency of the TM_{01} mode (or TM_{10} mode), while almost maintaining that of TM_{21} mode (or TM_{12} mode) to be unchanged. With these arrangements, a wide impedance bandwidth with stable radiation peak in the broadside direction is achieved for the MPA under this dual modes operation. Finally, the dual-polarized MPA is fabricated and measured. The measured results are found in good agreement with the simulated ones in terms of the reflection coefficient, radiation pattern, and realized gain, demonstrating that the MPA's impedance bandwidth ($|S_{dd11}| < -10$ dB) is tremendously increased up to about 8% with a high differential port-to-port isolation of better than 22.6 dB. In particular, a low profile property of about 0.024 free-space wavelength and the stable radiation pattern are also achieved.

INDEX TERMS Microstrip patch antenna, differential-fed, dual-polarized, bandwidth enhancement, low profile, radiation pattern transformation.

I. INTRODUCTION

Dual-polarized antennas have gained much attenuation in modern communications for the purpose of reducing multipath fading and enhancing channel capacity [1] and [2]. Meanwhile, the differential circuit has been increasingly demanded for communication systems due to its noise immunity, harmonic suppression, and large dynamic range [3] and [4]. However, the traditional dual-polarized antennas with a single feed in [5] and [6] should be connected with differential microwave circuits with virtue of an additional balun, which causes the extra loss and decreases the efficiency.

In order to address this critical issue, various differential-fed dual-polarized antennas [7]–[16] have been proposed in the past few years. In [7], a differential-fed cavity-backed microstrip patch antenna (MPA) was presented with independent tunings of both polarizations. However, it suffers from a narrow impedance bandwidth of about 1.8% arising from the intrinsic high-Q factor in the thin substrate with the height of about 0.02 λ_0 (λ_0 is the free space wavelength). To overcome this issue, the ground plane of a differential-driven MPA in [8] was reshaped as a square annular cavity towards exciting another resonance in proximity to its dominant mode, thus achieving an improved bandwidth of about 61%. But, the modified ground increases the profile of the MPA to about 0.24 λ_0.

Besides, the feeding scheme of the MPA could be improved for the wideband impedance matching. As reported in [9],

the feeding structure of the MPA had been reformed to widen its impedance bandwidth to about 68%. By employing a plate feeder in [10] and [11], the antennas generated a broad bandwidth of more than 67.5%. But, these antennas [9]–[11] inquire a high profile with the height of about 0.12 λ_0 or more, thus destroying their intrinsic low-profile or planar properties. Additionally, the radiating patch of this MPA could be reshaped to realize a wide-bandwidth performance. In [12], two pairs of double-layer U-shaped elements were adopted to yield a broad bandwidth of about 25.7%. The impedance bandwidth in [13] reached to about 113.2% by using the ring patch in combination with four triangular patches. Furthermore, it is an effective bandwidth-enhancement method by adding extra elements. In [14] and [15], four parasitic units were placed around the core radiator to gain a wide impedance bandwidth of more than 45%. The long dipoles in conjunction with the short dipoles in [16] were utilized to control the lower and higher resonant frequencies, respectively, leading to an enhanced bandwidth of about 45%. Nevertheless, all of these reported approaches [12]–[16] unexpectedly increase the complexity in antenna design. In [17], the impedance bandwidth of the dual-polarized antenna maintained about 9.5% by using four isolated micro patches. Whereas, the antenna has a high profile of about 0.07 λ_0.

Recently, the TM_{10} and TM_{30} modes of a differential-fed MPA in [18] were adopted for bandwidth improvement (13%) with a low profile property. However, the asymmetrical radiating patch is unsuitable to be chosen for a wide-band dual- polarized antenna. Based on the cavity model, the first and second odd-order modes of a square MPA, i.e., TM_{01} and TM_{21} modes (or TM_{10} and TM_{12} modes), are excited adjacent to each other. Unfortunately, the monopole-like H-plane radiation pattern of TM_{21} mode (or TM_{12} mode) [19] is unable to maintain its radiation peak in the broadside direction. To the best of our knowledge, no any work has been reported so far to transform the radiation pattern of TM_{21} mode into the broadside radiation, and then employ the dual modes to achieve a wideband bandwidth with the low profile property.

In this paper, a differential-fed dual-polarized MPA with improved bandwidth and low profile property under radiation of dual odd-order modes is proposed for the first time. Initially, a square MPA operating in TM_{21} mode is theoretically investigated. It is found that its radiated field has maxima off broadside and can be transformed into the broadside radiation by etching out a narrow slot at the center of the patch. Then, the resonant frequencies of the MPA loaded with shorting pins are extensively studied. The results demonstrate that the resonant frequency of TM_{01} mode (or TM_{10} mode) is gradually pushed up with slight effect on that of TM_{21} mode (or TM_{12} mode). With the use of this procedure, the dual odd-order modes are simultaneously excited to improve the bandwidth of the dual- polarized antenna with stable radiation patterns. After the extensive analysis is executed, the proposed MPA is fabricated and tested. The results illustrate that the antenna has gained an enhanced impedance bandwidth of about 8%, while maintaining a thin height of about 0.024 λ_0. Most importantly, a stable radiation pattern with its radiation peak in the broadside direction is satisfactorily performed over the operating band.

II. GEOMETRY AND ANALYSIS OF APERTURE-FED ANTENNA

Fig. 1 illustrates the configuration of the proposed differential-fed dual-polarized MPA. It consists of a square radiating patch, a ground plane, and an array of twenty-four shorting pins. The radiating patch with the length of W is formed on the top surface of the dielectric substrate ($\varepsilon_r = 2.2$ and $H = 1.542$ mm). The ground plane ($W_g \times W_g$) is located below the substrate with an air gap of H_1. Besides, an array of shorting pins is inserted between the radiating patch and ground plane for the purpose of reallocating the resonant frequency of the TM_{01} mode (or TM_{10} mode) in proximity to that of TM_{21} mode (or TM_{12} mode). Furthermore, a cross-shaped linear slot is etched out at the center of the square patch to transform the monopole-like radiation of TM_{21} mode (or TM_{12} mode) into the broadside radiation. Meanwhile, it contributes to the input inductance reduction caused by the pins and probes. In this context, the entire antenna with its detailed dimensions as tabulated in Table 1 is simulated and characterized by using the fullwave HFSS 13.0 simulator. Due to the symmetric geometry of the MPA in Fig. 1, only the differential-driven ports 1+ and 1− along the y-direction to excite the antenna in Fig. 2 are deeply studied in order to carry out our investigation simplistically.

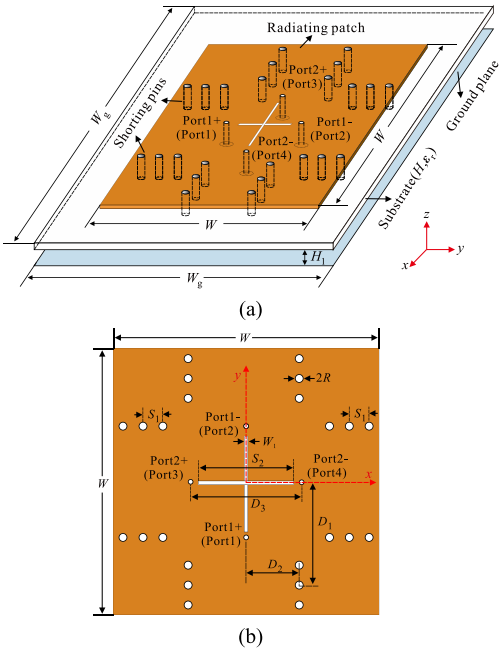

FIGURE 1. Geometry of the proposed wideband dual-polarized MPA loaded with the shorting pins and a cross-shaped slot. (a) 3D view. (b) Top view.

TABLE 1. Dimensions of dual-polarized antenna in fig. 1.

Parameters	W	W_1	W_g	D_1	D_2
Values(mm)	165	1.5	330	67.65	36.3
Parameters	D_3	S_1	S_2	H_1	R
Values(mm)	144	13	54.2	2.4	1.0

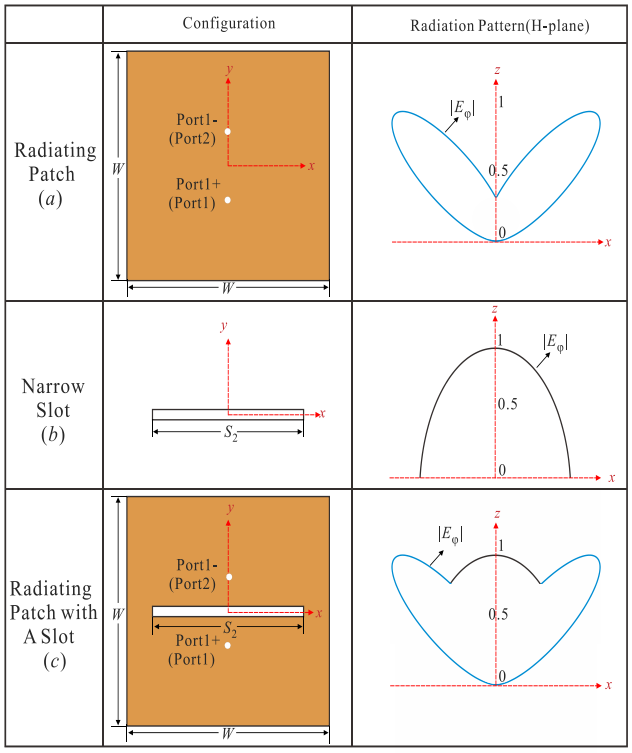

FIGURE 2. Radiation patterns of three distinctive antennas. (a) TM_{21} mode of the MPA. (b) Narrow slot. (c) TM_{21} mode of the MPA loaded with a slot.

A. REALIZATION OF BROADSIDE RADIATION OF TM_{21} MODE

Our effort in this section is made to transform the traditional monopole-like radiation of TM_{21} mode into the broadside radiation, so as to achieve a wide bandwidth with stable radiation patterns with the combination of TM_{01} mode.

Based on the cavity model [20], the radiation patterns of a square MPA in Fig. 2 (a) can be calculated by modeling the antenna as the two-element array of slots along the x-direction at $(H + H_1) \ll \lambda_0$. Since then, the equivalent magnetic current densities across these slots are expressed as

$$\vec{M_s} = \vec{E} \times \vec{n} \tag{1}$$

With resorting to the aperture antenna theory, the normalized far-zone electric field of the MPA under radiation of TM_{21} mode can be derived as

$$E_\theta = \frac{\cos(Y)X\sin(X)W\sin(\phi)}{\pi^2 - X^2} \tag{2}$$

$$E_\phi = \frac{\cos(Y)X\sin(X)W\cos(\theta)\cos(\phi)}{\pi^2 - X^2} \tag{3}$$

where k_0 is the wave number in free space, and

$$X = 0.5k_0W\sin(\theta)\cos(\phi) \tag{4}$$

$$Y = 0.5k_0W\sin(\theta)\sin(\phi) \tag{5}$$

Therefore, the H-plane (xz-plane) radiation pattern of the MPA under TM_{21} mode can be simplified as a function of the polar angle (θ)

$$E_\phi = \frac{(0.5k_0W\sin(\theta))\sin(0.5k_0W\sin(\theta))W\cos(\theta)}{\pi^2 - (0.5k_0W\sin(\theta))^2} \tag{6}$$

For the slot along the x-direction in Fig. 2 (b), the previous works in [21] and [22] had demonstrated that its H-plane radiation pattern over the upper half space can be given as

$$E_\phi = \frac{\sin(0.5k_0S_2\sin(\theta))\cos(\theta)}{0.5k_0S_2\sin(\theta)} \tag{7}$$

By using (6) and (7), we can figure out the normalized H-plane radiation pattern of the MPA and slot as depicted in Fig. 2 (a) and (b), respectively. It can be obviously seen that the traditional MPA operating in TM_{21} mode has a null in the broadside direction, which is unsuitable to be combined with the TM_{01} mode to achieve an enhanced bandwidth with stable broadside radiation patterns. Coincidentally, the slot aperture in Fig. 2 (b) maintains its radiation peak in the broadside direction. Therefore, if the radiated field from the central slot is gradually strengthened for the improved MPA in Fig. 2 (c), a broadside radiation pattern of the TM_{21} mode can be realized. The previous work in [22] illustrates that one of the most effective ways to enhance the slot radiation is to increase its length S_2.

In order to explain the above operating principle in detail, the simulated radiation patterns of the MPA (Fig. 2 (c)) under TM_{21} mode at $S_2/W = 0$, 0.2, 0.3, and 0.4 are further studied and the relevant results are plotted in Fig. 3. When the slot is not etched out on the radiating patch or $S_2/W = 0$, the monopole-like radiation pattern is performed for the traditional MPA. But, as S_2 increases from 0 to 0.4 W, the main radiation is performed in the broadside direction ($\theta = 0°$) gradually due to the increased radiated field from the central slot. After S_2 reaches to about 0.4 W, the monopole-like radiation of TM_{21} mode is successfully transformed into the broadside radiation.

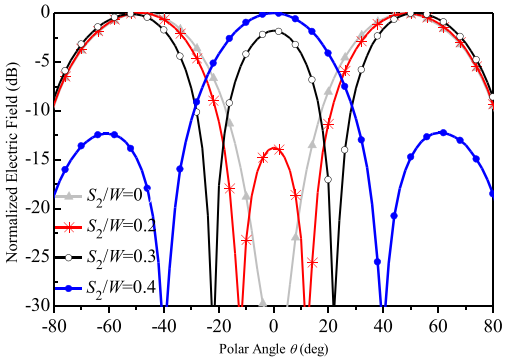

FIGURE 3. Simulated electric field of the MPA in Fig. 2 (c) on an infinite ground plane operating in TM_{21} mode under different slot length S_2.

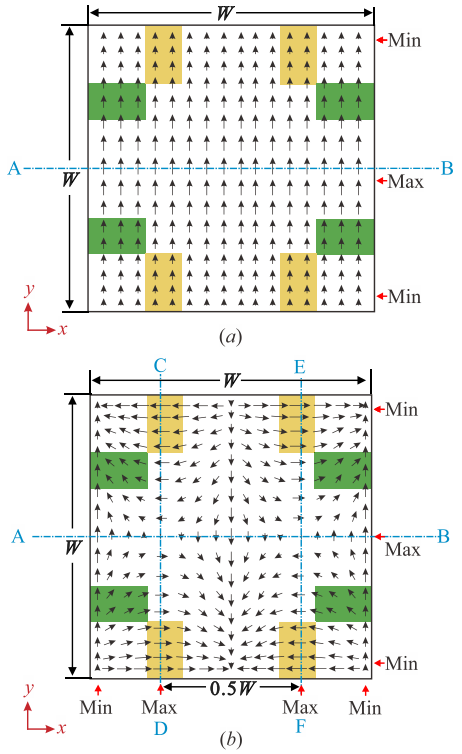

FIGURE 4. Surface current density distributions of the MPA under different resonant modes. (a) TM_{01} mode. (b) TM_{21} mode.

B. ELECTRIC CURRENT DISTRIBUTIONS UNDER DUAL RADIATIVE MODES

Next, let us sketch the surface current density distribution on the radiating patch under the operating of TM_{01} and TM_{21} modes in Fig. 4 in order to select the position of shorting pins properly for the realization of a wideband antenna. Looking at Fig. 4 (a), the magnitude of current distribution of the TM_{01} mode keeps almost constant along the x-direction, whereas, it is gradually increased from the edge of the patch to its central plane (AB) along the y-direction. With respect to the current distribution of the TM_{21} mode in Fig. 4 (b), it has the similar tendency along the y-direction. However, the magnitude of current distributions has two maximum values in the x-direction (CD- and EF- plane), which keeps a distance of around 0.25 W to the center of the patch. Within the yellow region, the strongest and weakest current distributions are performed for the TM_{21} and TM_{01} modes, respectively. Therefore, the shorting pins should be loaded around this region to push up the resonant frequency of TM_{01} mode (f_{01}) of the MPA in proximity to that of TM_{21} mode (f_{21}) for realizing a wide impedance bandwidth. Similarly, the shorting pins are added around the green region to excite another polarization under the operation of TM_{10} and TM_{12} modes.

III. PARAMETRIC STUDY AND DESIGN OF PROPOSED ANTENNA

Based on the working principle described above, it can be well understood that the proposed approach is presented to reshape the radiation pattern of TM_{21} mode and describe the detail region by inserting pins to reallocate the dual modes. To further investigate how the dimensional parameters influence the TM_{01} and TM_{21} modes of the MPA, each of the aforementioned parameters is distinctively studied under other parameters to be fixed.

A. SQUARE MPA LOADED WITH EIGHT SHORTING PINS

To start with, Fig. 5 shows the effect of two key parameters (D_1 and D_2) on the resonant frequencies (f_{21} and f_{01}) of a square MPA loaded with an array of eight shorting pins. As depicted in Fig. 5 (a), the f_{21}/f_{01} is always decreased firstly and then raised up by enlarging D_1 from 0.30 W to 0.48 W under three different values of D_2/W. Specifically, the antenna always obtains a lowest f_{21}/f_{01} by selecting $D_1/W + D_2/W = 0.64$. Under this condition, the f_{21}, f_{01}, and f_{21}/f_{01} of the MPA as a function of D_2/W are plotted in Fig. 5 (b). It can be seen that the f_{21} keeps nearly a constant value of about 1.82 GHz, whereas the f_{01} firstly raises up to a maximum value of 1.32 GHz at $D_1/W = 0.41$ and $D_2/W = 0.23$, and then falls down. Thus, a minimum f_{21}/f_{01} of about 1.38 is generated with the help of eight shorting pins.

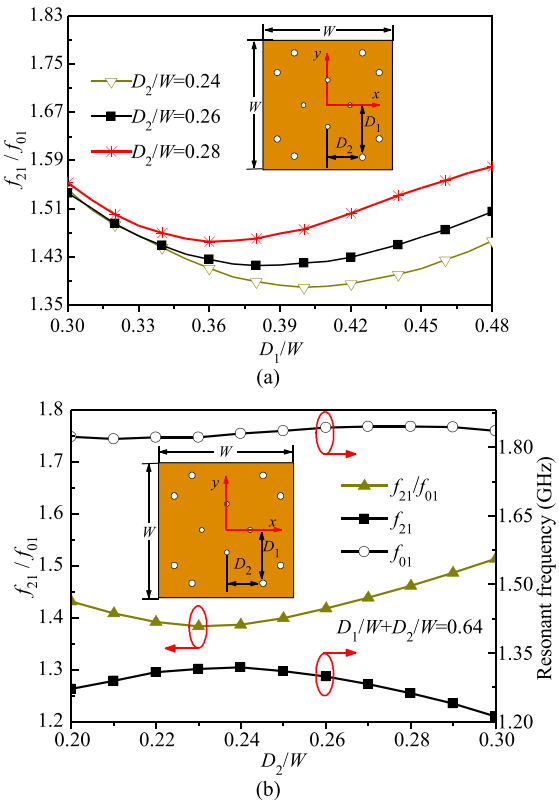

FIGURE 5. Two resonant frequencies and their frequency ratio (f_{21}/f_{01}) of the MPA loaded with eight pins as a function of two key parameters. (a) D_1/W. (b) D_2/W.

B. SQUARE MPA LOADED WITH SIXTEEN SHORTING PINS

In order to reallocate the dual modes more closely to each other, the resonant frequency of a square MPA loaded with sixteen shorting pins is further studied in Figs. 6 and 7 with

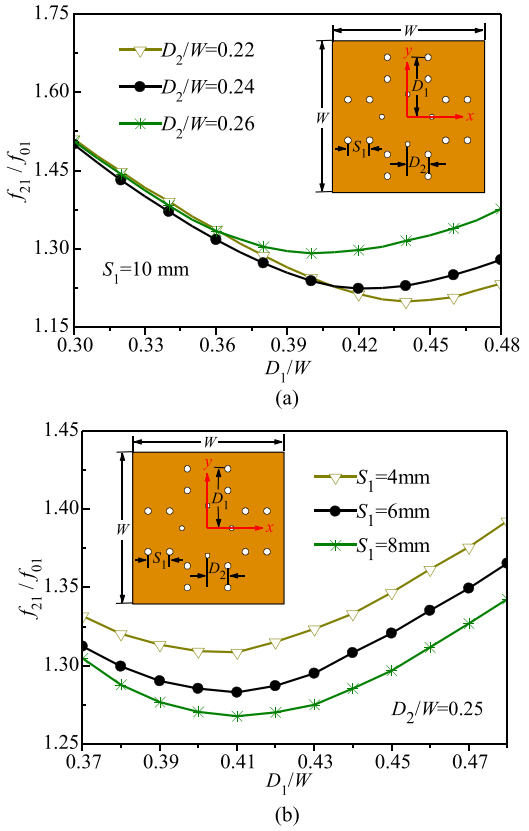

FIGURE 6. Frequency ratio (f_{21}/f_{01}) of the MPA loaded with sixteen pins as a function of D_1/W under different key parameters. (a) D_2/W. (b) S_1.

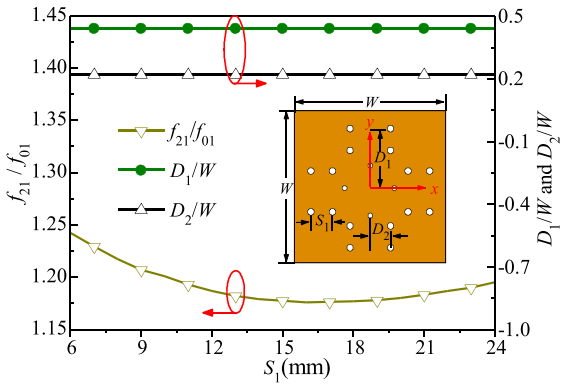

FIGURE 7. Frequency ratio f_{21}/f_{01}, D_1/W, and D_2/W of the MPA loaded with sixteen pins as a function of S_1.

regard to three critical parameters (D_1, D_2, and S_1). Initially, the f_{21}/f_{01} as a function of D_1/W under three different values of D_2/W at$S_1 = 10$ mm is analyzed and the relevant results are presented in Fig. 6 (a). It is found that the f_{21}/f_{01} goes down first and then rebounds. Meanwhile, the MPA acquires a lowest f_{21}/f_{01} under $D_1/W + D_2/W = 0.66$, which is similar to the tendency performed in Fig. 5 (a). After that, the influence of S_1 on the frequency ratio against D_1/W at $D_2/W = 0.25$ is illustrated in Fig. 6 (b). It shows that the lowest f_{21}/f_{01} is always obtained at $D_1/W = 0.41$. Based on the above analysis, Fig. 7 investigates the f_{21}/f_{01} as a function

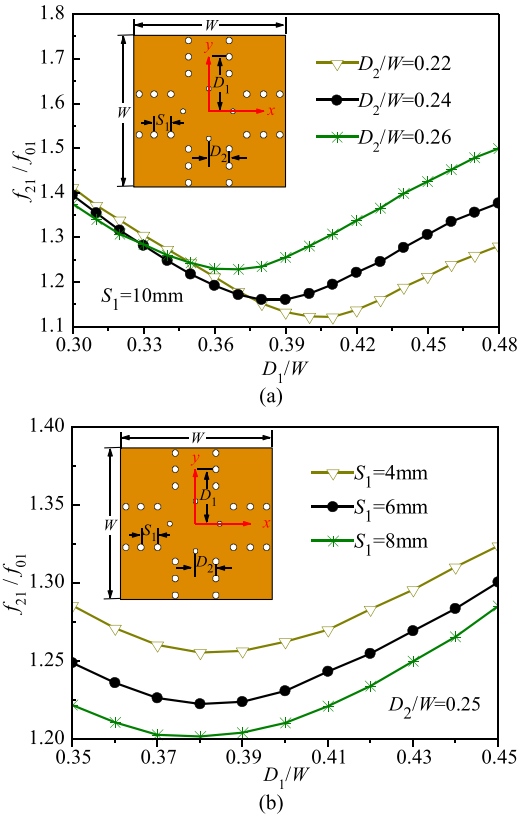

FIGURE 8. Frequency ratio (f_{21}/f_{01}) the MPA loaded with twenty-four pins as a function of D_1/W under different key parameters. (a) D_2/W. (b) S_1.

of S_1 with $D_1/W + D_2/W = 0.66$. The simulated results give us a hint that the minimum f_{21}/f_{01} for the MPA loaded with sixteen pins can be reduced to about 1.18 by setting D_1, D_2, and S_1 as 0.44 W, 0.22 W, 16 mm, respectively.

C. SQUARE MPA LOADED WITH TWENTY-FOUR SHORTING PINS

Although the f_{21}/f_{01} is already decreased to about 1.18 with the help of sixteen pins, the spacing in resonant frequency between the dual modes is still too far away to improve its bandwidth. Finally, an array of twenty-four pins is installed below the radiating patch as depicted in Figs. 8 and 9. Compared to the simulated results in Fig. 6, similar performances have occurred in Fig. 8. Herein, $D_1/W + D_2/W$ is selected as 0.63 to acquire the lowest frequency ratio as plotted in Fig. 9. The results suggest us that the lowest f_{21}/f_{01} of about 1.08 is generated by choosing D_1, D_2, and S_1 as 0.41 W, 0.22 W, and 13 mm, respectively, and it is located around the yellow and green regions as demonstrated in section II. Thus, a small green loop is produced in the upper part of the Smith Chart in Fig. 10.

D. INDUCTANCE REDUCTION FOR IMPEDANCE MATCHING

Unfortunately, the position of this green loop indicates that the image part of the input impedance is larger than 0 in a frequency range under the dual odd-order modes. With virtue

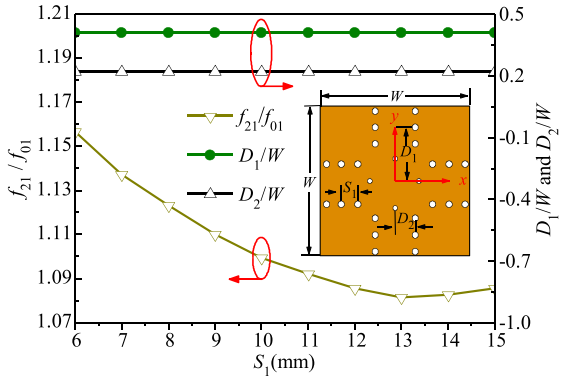

FIGURE 9. Frequency ratio f_{21}/f_{01}, D_1/W, and D_2/W of the MPA loaded with twenty-four pins as a function of S_1.

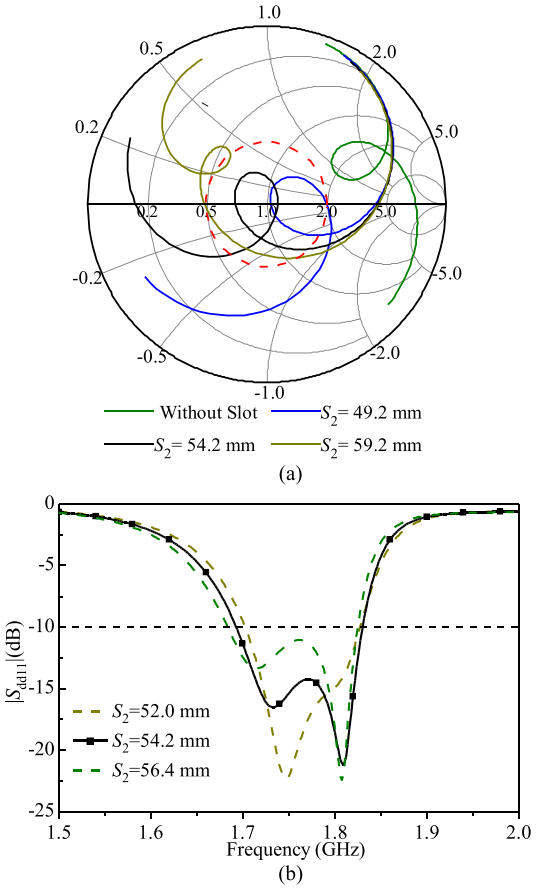

FIGURE 10. Impedance characteristics of the proposed MPA in Fig. 1 with respect to the slot length S_2. (a) Smith Chart. (b) $|S_{dd11}|$.

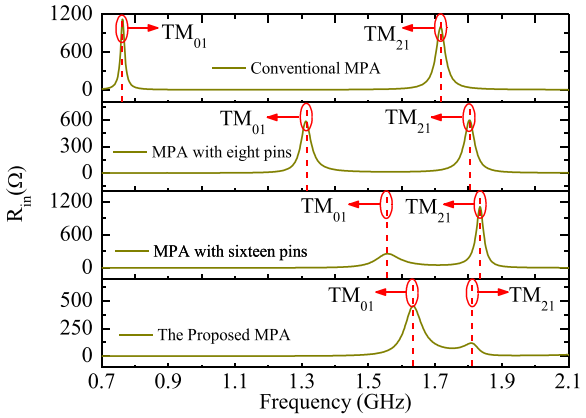

FIGURE 11. Migration of resonant frequencies of TM_{01} and TM_{21} modes under four distinctive MPAs.

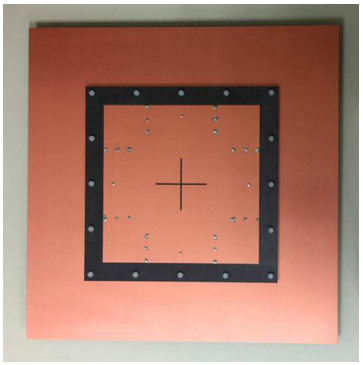

FIGURE 12. Photograph of the fabricated dual-polarized MPA.

of the slot, it not only transforms the radiation pattern of TM_{21} mode but also contributes to the equivalent inductance reduction [18]. Thus, the reflection coefficient of the MPA loaded with shorting pins and a cross-shaped slot in Fig. 1 is extensively studied in Fig. 10. As illustrated in Fig. 10 (a), the small loop is gradually moved down to the center of the Smith Chart. Thus, the inductance caused by the shorting pins and probes is effectively reduced by adding this slot. To illustrate the effect of the length S_2 on the $|S_{dd11}|$, the reflection coefficient as a function of frequency under three different lengths S_2 is presented in Fig. 10 (b). When the S_2 is chosen as 54.2 mm, a wide bandwidth is achieved with improved in-band performance.

Finally, the resonant frequency of the MPA under different conditions is plotted in Fig. 11 so as to explain the tendency about f_{21} and f_{01}. It can be observed herein that the f_{21} remains a constant of around 1.82 GHz, while the f_{01} is gradually pushed up. This tendency is mainly caused by the shorting pins loaded around the weakest current distribution of TM_{01} mode as studied in section II and previous works [23] and [24]. Under this condition, the size of the radiating patch of the MPA is increased to about 1.0 λ_0 × 1.0 λ_0.

IV. RESULTS AND DISCUSSION

To validate the operating principle and attractive features of the proposed MPA with bandwidth enhancement under dual resonances, the differential-fed dual-polarized MPA loaded with an array of twenty-four shorting pins and a cross-shaped slot is designed and fabricated. The top-view photography of the fabricated patch antenna is displayed in Fig. 12.

As shown in Fig. 1, four single ended ports 1, 2, 3 and 4 are used to realize two differential ports of 1+, 1− and 2+, and 2−, respectively. Therefore, the differential S-parameters

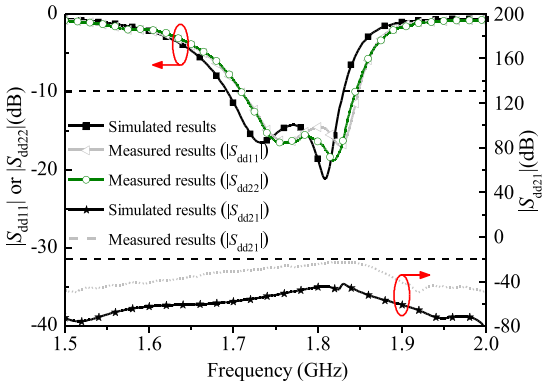

FIGURE 13. Simulated and measured differential S-parameters of the proposed dual-polarized MPA.

($|S_{dd11}|$, $|S_{dd22}|$, $|S_{dd21}|$, and $|S_{dd12}|$) of the proposed wideband MPA can be defined as [9].

$$S_{dd11} = (S_{11} - S_{12} - S_{21} + S_{22})/2 \quad (8)$$

$$S_{dd22} = (S_{33} - S_{34} - S_{43} + S_{44})/2 \quad (9)$$

$$S_{dd21} = (S_{31} - S_{41} - S_{32} + S_{42})/2 \quad (10)$$

$$S_{dd12} = (S_{13} - S_{14} - S_{23} + S_{24})/2 \quad (11)$$

where S_{ij} (i = 1, 2, 3, 4; j = 1, 2, 3, 4) is the single-ended S-parameters when the differentially-fed dual-polarized antenna is regarded as a single-ended 4-port network.

By using the R & S ZNB20 Vector Network Analyzer, the differential S-parameters are measured as depicted in Fig. 13. Notice that the measured results with dual attenuation poles are in good agreement with the simulated ones. On one hand, the fabricated differential-fed MPA achieves an enhanced impedance bandwidth for $|S_{dd11}|$ (or $|S_{dd22}|$) of about 8% ranging from 1.71 to 1.85 GHz with low profile property of about 0.024 λ_0. On the other hand, the transmission coefficient between differential-fed ports 1 and 2 ($|S_{dd21}|$ and $|S_{dd12}|$) of less than −22.6 dB is obtained over the operating band, thus indicating a good isolation between the differential-driven ports.

With respect to the radiation patterns and gain, both of them are measured by adopting the near-field SATIMO antenna test system. In our work, a wideband 180° power divider ZAPDJ-2 from Mini-Circuits is used to transform the single-ended signal to the differential signal. When the radiation patterns of differential-fed port 1 were measured, the two output ports of the 180° hybrid coupler were connected to ports 1+ and 1−, respectively, while ports 2+ and 2− were connected with two 50 Ω loads. Due to the symmetric geometry, only the radiation characteristic of the MPA under the differential-fed port 1 are investigated as illustrated in Fig. 14. It can be seen that good agreement between the simulated and measured results is exhibited in the *xz*- and *yz*-plane. Besides, a stable radiation pattern with the same polarization is satisfactorily achieved wihin the operating band. With respect to the large E-plane sidelobe, the previous work [25]

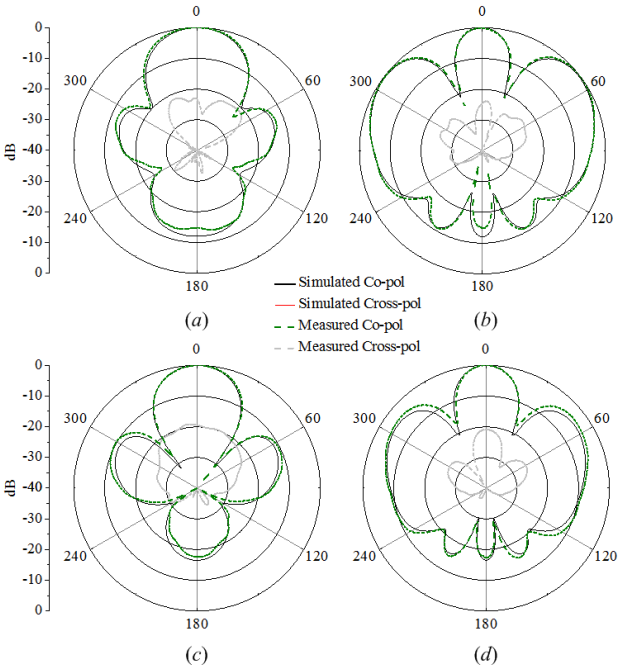

FIGURE 14. Simulated and measured radiation patterns of the proposed dual-polarized MPA at differential-fed port 1. (a) *xz*-plane at 1.72 GHz; (b) *yz*-plane at 1.72 GHz; (c) *xz*-plane at 1.81 GHz; (d) *yz*-plane at 1.81 GHz.

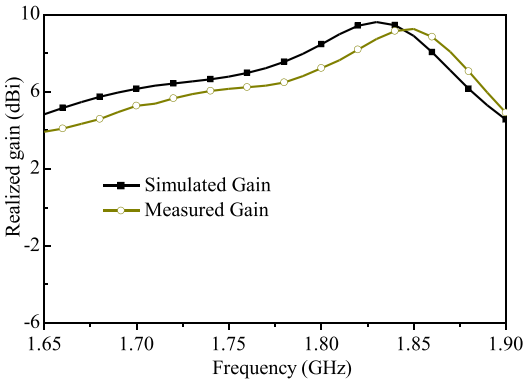

FIGURE 15. Simulated and measured radiation gains of the proposed dual-polarized MPA at differential-fed port 1.

demonstrate the electric length between the dual equivalent magnetic currents are properly enlarged to about 0.62 λ_0 so as to achieve an enhanced Gain for the MPA. However, in our work, the electric length is dramatically increased to about 1.0 λ_0, resulting to producing a big sidelobe level of E-plane radiation patterns. Fig. 15 presents the simulated and measured gains as a function of frequency. A reasonably stable gain of around 7 dBi at the broadside direction is obtained over the entire operating band.

V. CONCLUSION

In this paper, a low-profile wideband differential-fed dual-polarized MPA under radiation of dual odd-order modes is proposed. Firstly, the radiation pattern of the TM_{21} mode

for the MPA loaded with a slot is deeply analyzed. The results demonstrate that its monopole-like radiation pattern can be reshaped as the broadside radiation by increasing the slot length. Secondly, the influence of different numbers of shorting pins on the resonant frequency of the MPA is extensively studied. The simulated results suggest us that an array of twenty-four shorting pins should be properly inserted below the radiating patch, so as to push up the f_{01} in proximity to the f_{21}. With this arrangement, a wide impedance bandwidth with stable radiation patterns is obtained for the dual-polarized MPA. In final, the proposed antenna is fabricated and tested. The measured results show that this proposed planar MPA has achieved an enhanced bandwidth of about 8%. Particularly, a small height of about 0.024 λ_0 with stable normal radiation patterns is maintained as well to demonstrate its performance as highly demanded in all the planar antennas.

REFERENCES

[1] K.-L. Wong, *Compact and Broadband Microstrip Antennas*. New York, NY, USA: Wiley, 2002.

[2] D.-Z. Zheng and Q.-X. Chu, "A multimode wideband ±45° dual-polarized antenna with embedded loops," *IEEE Antennas Wireless Propag. Lett.*, vol. 16, pp. 633–636, 2017.

[3] Y. P. Zhang, J. J. Wang, Q. Li, and X. J. Li, "Antenna-in-package and transmit-receive switch for single-chip radio transceivers of differential architecture," *IEEE Trans. Circuits Syst. I, Reg. Papers*, vol. 55, no. 11, pp. 3564–3570, Dec. 2008.

[4] W. R. Eisenstadt, B. Stengel, and B. M. Thompson, *Microwave Differential Circuit Design Using Mixed-Mode S-Parameters*. Boston, MA, USA: Artech House, 2006.

[5] C.-X. Mao, S. Gao, Y. Wang, F. Qin, and Q.-X. Chu, "Multimode resonator-fed dual-polarized antenna array with enhanced bandwidth and selectivity," *IEEE Trans. Antennas Propag.*, vol. 63, no. 12, pp. 5492–5499, Dec. 2015.

[6] S.-W. Wong, Q.-K. Huang, G.-H. Sun, L. Zhu, and Q.-X. Chu, "Multiple-mode wideband dual-polarized antenna for long term evolution (LTE) application," *IEEE Antennas Wireless Propag. Lett.*, vol. 15, pp. 203–206, 2016.

[7] C. R. White and G. M. Rebeiz, "A differential dual-polarized cavity-backed microstrip patch antenna with independent frequency tuning," *IEEE Trans. Antennas Propag.*, vol. 58, no. 11, pp. 3490–3498, Nov. 2010.

[8] D. Sun, Z. Zhang, X. Yan, and X. Jiang, "Design of broadband dual-polarized patch antenna with backed square annular cavity," *IEEE Trans. Antennas Propag.*, vol. 64, no. 1, pp. 43–52, Jan. 2016.

[9] Q. Xue, S. W. Liao, and J. H. Xu, "A differentially-driven dual-polarized magneto-electric dipole antenna," *IEEE Trans. Antennas Propag.*, vol. 61, no. 1, pp. 425–430, Jan. 2013.

[10] F. Zhu *et al.*, "Ultra-wideband dual-polarized patch antenna with four capacitively coupled feeds," *IEEE Trans. Antennas Propag.*, vol. 62, no. 5, pp. 2440–2449, May 2014.

[11] Y.-Y. Liu and Z.-H. Tu, "Differential enhanced broadband dual-polarized printed dipole antenna for base stations," *Microw. Opt. Technol. Lett.*, vol. 58, no. 12, pp. 2864–2868, Dec. 2016.

[12] B. Feng, S. Li, W. An, W. Hong, and S. Yin, "A differentially driven dual-polarized dual-wideband complementary antenna for 2G/3G/LTE applications," *Int. J. Antennas Propag.*, vol. 2014, Jun. 2014, Art. no. 480268.

[13] K. Zhang, F. G. Zhu, and S. Gao, "Differential-fed ultra-wideband slot-loaded patch antenna with dual orthogonal polarisation," *Electron. Lett.*, vol. 49, no. 25, pp. 1591–1593, Dec. 2013.

[14] Y. Cui, X. Gao, and R. Li, "A broadband differentially fed dual-polarized planar antenna," *IEEE Trans. Antennas and Propag.*, vol. 65, no. 6, pp. 3231–3234, Jun. 2017.

[15] D.-L. Wen, D.-Z. Zheng, and Q.-X. Chu, "A wideband differentially fed dual-polarized antenna with stable radiation pattern for base stations," *IEEE Trans. Antennas Propag.*, vol. 65, no. 5, pp. 2248–2255, May 2017.

[16] Y. Luo and Q.-X. Chu, "Oriental crown-shaped differentially fed dual-polarized multidipole antenna," *IEEE Trans. Antennas Propag.*, vol. 63, no. 11, pp. 4678–4685, Nov. 2015.

[17] X. Chen, P.-Y. Qin, Y. J. Guo, and G. Fu, "Low-profile and wide-beamwidth dual-polarized distributed microstrip antenna," *IEEE Access*, vol. 5, pp. 2272–2280, Jan. 2017.

[18] N.-W. Liu, L. Zhu, and W.-W. Choi, "A differential-fed microstrip patch antenna with bandwidth enhancement under operation of TM_{10} and TM_{30} modes," *IEEE Trans. Antennas Propag.*, vol. 65, no. 4, pp. 1607–1614, Apr. 2017.

[19] P. Hammer, D. Van Bouchaute, D. Verschraeven, and A. Van de Capelle, "A model for calculating the radiation field of microstrip antennas," *IEEE Trans. Antennas Propag.*, vol. 27, no. 2, pp. 267–270, Mar. 1979.

[20] R. Garg, P. Bhartia, I. Bahl, and A. Ittipiboon, *Microstrip Antenna Design Handbook*. Boston, MA, USA: Artech House, 2001.

[21] C. A. Balanis, *Antenna Theory: Analysis and Design*. Hoboken, NJ, USA: Wiley, 2005.

[22] P. Juyal and L. Shafai, "Sidelobe reduction of TM_{12} mode of circular patch via nonresonant narrow slot," *IEEE Trans. Antennas Propag.*, vol. 64, no. 8, pp. 3361–3369, Aug. 2016.

[23] B. Wang and Y. Lo, "Microstrip antennas for dual-frequency operation," *IEEE Trans. Antennas Propag.*, vol. 32, no. 9, pp. 938–943, Sep. 1984.

[24] S. S. Zhong and Y. T. Lo, "Single-element rectangular microstrip antenna for dual-frequency operation," *Electron. Lett.*, vol. 19, no. 8, pp. 298–300, Apr. 1983.

[25] X. Zhang and L. Zhu, "Gain-enhanced patch antennas with loading of shorting pins," *IEEE Trans. Antennas Propag.*, vol. 64, no. 8, pp. 3310–3318, Aug. 2016.

NENG-WU LIU (S'15) was born in Changde, China. He received the B.S and M.E degrees in electrical engineering from Xidian University, Xi'an, China, in 2012 and 2015, respectively. He is currently pursuing the Ph.D. degree in electrical and computer engineering with the University of Macau. His research interest focuses on wideband antennas and circularly polarized antennas.

Mr. Liu was the recipient of the Best Student Paper Award of the 2016 IEEE 17th Macau/HK AP/MTT Postgraduate Conference.

LEI ZHU (S'91–M'93–SM'00–F'12) received the B.Eng. and M.Eng. degrees in radio engineering from the Southeast University, Nanjing, China, in 1985 and 1988, respectively, and the Ph.D. degree in electronic engineering from the University of Electro-Communications, Tokyo, Japan, in 1993.

From 1993 to 1996, he was a Research Engineer with Matsushita-Kotobuki Electronics Industries Ltd., Tokyo, Japan. From 1996 to 2000, he was a Research Fellow with the École Polytechnique de Montréal, Montréal, QC, Canada. From 2000 to 2013, he was an Associate Professor with the School of Electrical and Electronic Engineering, Nanyang Technological University, Singapore. In 2013, he joined the as a Full Professor with Faculty of Science and Technology, University of Macau, Macau, China, where he has been a Distinguished Professor since 2016. From 2014 to 2017, he served as the Head of Department of Electrical and Computer Engineering, University of Macau. He has authored or co-authored over 380 papers in international journals and conference proceedings. His papers have been cited over 4700 times with the H-index of 38 (source: ISI Web of Science). His research interests include microwave circuits, guided-wave periodic structures, planar antennas, and computational electromagnetic techniques.

Dr. Zhu served as the member of the IEEE MTT-S Fellow Evaluation Committee (2013–2015). He has been serving as the member of IEEE AP-S Fellows Committee (2015–2017). He was the recipient of the 1997 Asia–Pacific Microwave Prize Award, the 1996 Silver Award of Excellent Invention from Matsushita-Kotobuki Electronics Industries Ltd., and the 1993 First-Order Achievement Award in Science and Technology from the National Education Committee, China. He served as a General Chair of the 2008 IEEE MTT-S International Microwave Workshop Series on the Art of Miniaturizing RF and Microwave Passive Components, Chengdu, China, and a Technical Program Committee Co-Chair of the 2009 Asia–Pacific Microwave Conference, Singapore. He was an Associate Editor for the IEEE TRANSACTIONS ON MICROWAVE THEORY AND TECHNIQUES (2010–2013) and IEEE MICROWAVE AND WIRELESS COMPONENTS LETTERS (2006–2012).

XIAO ZHANG (S'15) was born in Gaozhou, Guangdong, China. He received the B.Eng. degree in information engineering and the M.Eng. degree in communication and information systems from South China University of Technology, Guangzhou, Guangdong, China, in 2011 and 2014, respectively. Currently, he is currently pursuing the Ph.D. degree with the University of Macau. His research interest includes microwave.

WAI-WA CHOI (M'00–SM'10) was born in Macau in 1970. He received the B.Sc., M.Sc., and Ph.D. degrees in electrical and electronics engineering from the University of Macau, Macau, China, in 1993, 1997, and 2008, respectively.

From 1993 to 1995, he was a Research Assistant with the Institute of Systems and Computer Engineering, Lisbon, Portugal. Since 1995, he has been with the University of Macau, Macau, China, where he is currently an Associate Professor with the Department of Electrical of Computer Engineering. He has authored or co-authored over 40 internationally refereed journal and conference papers. His research interests are in the areas of microwave active and passive circuits, smart antennas, radar, and RFID systems.

Dr. Choi has served as a reviewer for the IEEE TRANSACTIONS ON MICROWAVE THEORY AND TECHNIQUES, the IEEE TRANSACTIONS ON INDUSTRIAL ELECTRONICS, IEEE MICROWAVE AND WIRELESS COMPONENTS LETTERS, and IEEE ANTENNAS AND WIRELESS PROPAGATION LETTERS. Since 2015, He has been the Chair of IEEE MACAU ANTENNAS AND PROPAGATION MICROWAVE THEORY AND TECHNIQUES JOINT CHAPTER.